Conf-920677--16

Results From A Large-Scale MHD Propulsion Experiment

M. Petrick* , J. Libera, J.X. Bouillard, E.S. Pierson and D. Hill
Argonne National Laboratory
Argonne, IL 60439

ANL/CP--76633

DE92 018177

ABSTRACT

Background

Magnetohydrodynamic (MHD) thrusters have long been recognized as potentially attractive candidates for ship propulsion because such systems eliminate the conventional rotating drive components. The MHD thruster is essentially an electromagnetic (EM) pump operating in seawater. An electrical current is passed directly through the seawater and interacts with an applied magnetic field; the interaction of the magnetic field and the electrode current in the seawater results in a Lorentz force acting on the water, and the reaction to this force propels the vessel forward.

The concept of EM propulsion has been examined periodically during the past 35 years as an alternative method of propulsion for surface ships and submersibles. The conclusions reached in early studies were that MHD thrusters restricted to fields of 2 T (the state-of-the-art at that time) were impractical and very inefficient. With the evolution of superconducting magnet technology, later studies investigated the performance of MHD thrusters with much higher magnetic field strengths and concluded that at higher fields (>6-T) practical MHD propulsion systems appear possible. The feasibility of attaining the requisite higher magnetic fields has increased markedly because of rapid advances in building high-field superconducting magnets and the recent evolution of high-temperature superconductors.

ANL Program

Argonne National Laboratory (ANL) is conducting a large-scale MHD propulsion experiment using an existing 6 Tesla superconducting magnet that was developed by the Department of Energy (DOE) in the 1970's. The 180 ton, 13 foot diameter, dipole superconducting magnet has been installed in a unique 75 foot long seawater test facility built specifically for the experimental program. The objectives of the program are: (1) Development of a fundamental understanding of generic MHD- and electrolysis-related phenomena that can affect the performance of MHD thrusters; (2) Development of a validated analytical capability (models, scaling factors, et cetera) that can be used to predict the performance of full-scale MHD thrusters over the operational parametric ranges of interest; (3) Generation of a database relative to the critical MHD loss mechanism that can be utilized to support the design and/or evaluation of various MHD thruster configurations.

The experimental program has been structured to focus on and investigate the generic MHD phenomena (loss mechanisms) that can adversely affect MHD thruster performance. The individual tests have been designed to verify predicted changes in thruster performance and, where possible, isolate and quantify individual loss mechanisms. The key independent thruster operating parameters that have been investigated are (1)

DISTRIBUTION OF THIS DOCUMENT IS UNLIMITED

* Paper presenter

MASTER

The submitted manuscript has been authored by a contractor of the U. S. Government under contract No. W-31-109-ENG-38. Accordingly, the U. S. Government retains a nonexclusive, royalty-free license to publish or reproduce the published form of this contribution, or allow others to do so, for U. S. Government purposes.

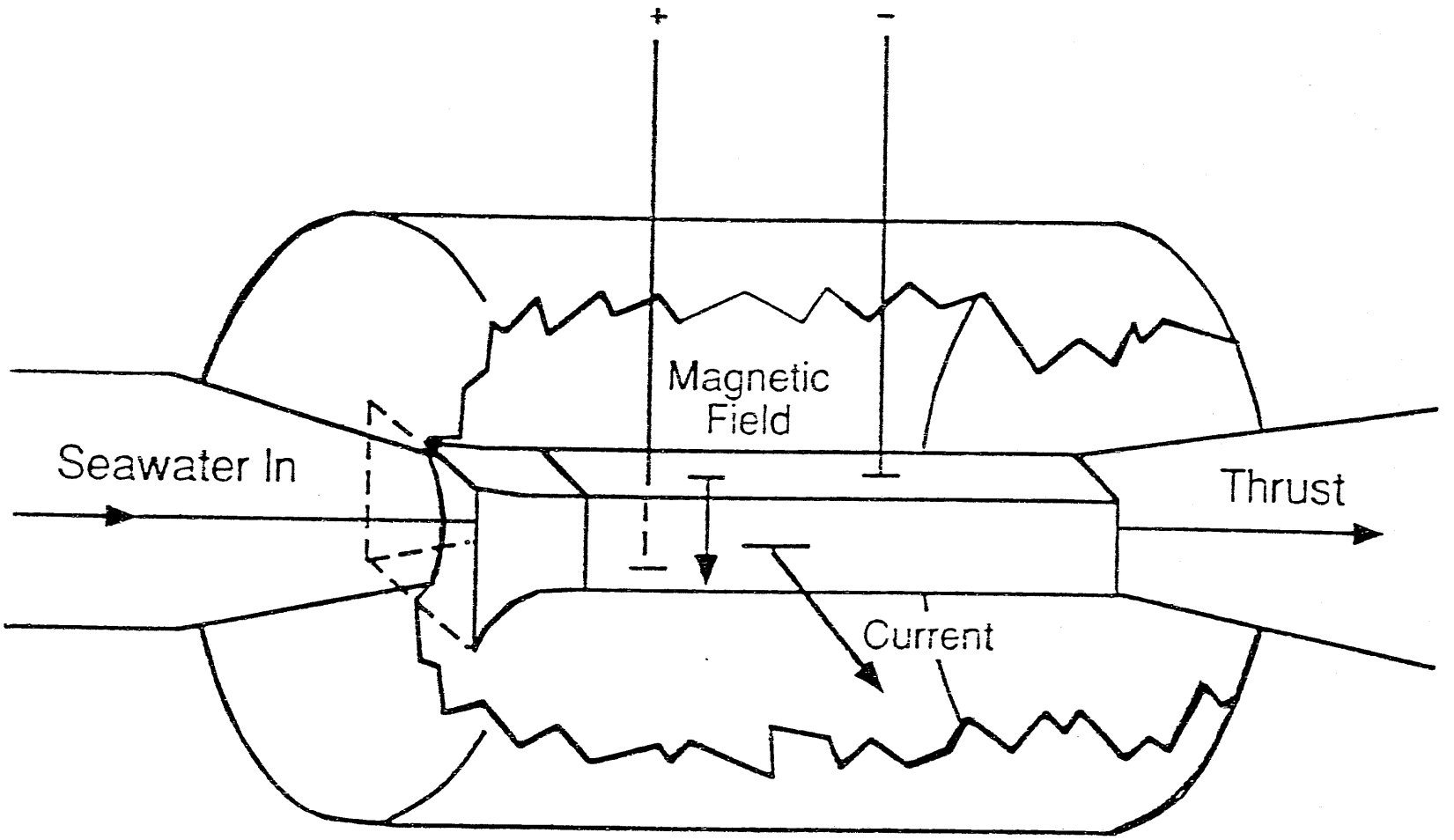

Fig. 1.0. MHD Thruster

magnetic field, 1 to 6 Tesla; (2) thruster electrical load factor (a measure of current density), 1.5 to 5.0; and (3) pressure, 15 to 200 psi.

To aid the experimental program design as well as data correlation and interpretation, both dimensional analysis and 3-D modeling has been pursued. The 3-D models developed have provided the physical insights and fundamental understanding required to provide a sound basis and/or guidance for projecting performance to full-scale thrusters.

Experimental Results

The test thruster and facility have become operational, following an indepth check-out period. Data acquisition is underway and analyses of the data has been initiated. The limited analyses completed thus far indicates good agreement between measured and predicted values. In addition, isolation and quantification of individual losses such as anode and cathode over voltages (electrode drops), end currents, friction factors, etc. as a function of the key independent operating parameters has been achieved. The experimental results will be presented and discussed during the presentation.

NOMENCLATURE

K	Thruster load factor,
U_p	Velocity of water in MHD thruster,
C_D	Drag coefficient of ship,
U_s	Velocity of ship,
D_s	"Effective" diameter of ship,
ρ	Density of seawater,
L_s	Length of ship,
σ	Electrical conductivity of seawater,
D_T	Equivalent diameter of MHD thruster cross section,
B	Magnetic flux density,
L_T	Length of thruster, and
η_T	Overall efficiency of MHD thruster.
K_L	Local load factor
K_o	Center line along the flow load factor
E	Local electric field intensity
U	Local flow velocity
B_o	Magnetic flux density at center of thruster
$\overline{U}$	Average flow velocity
V_t	Terminal (electrode) voltage difference
a	Electrode separation
d	The channel half width parallel to $\overline{B}_o$
μ	The seawater viscosity

INTRODUCTION

Magnetohydrodynamic (MHD) thrusters have long been recognized as potentially attractive candidates for ship propulsion because such systems eliminate the conventional rotating drive components. The MHD thruster schematically illustrated in Fig. 1 is an electromagnetic (EM) pump operating in seawater. An electrical current is passed directly through the seawater and interacts with an applied magnetic field; the interaction of the magnetic field and the electric current in the seawater results in a Lorentz force acting on the

water; the reaction to this force propels the vessel forward. The EM thruster thus replaces the conventional shaft-gear-propeller system.

The principal issues in regard to MHD thrusters do not include feasibility, since electromagnetic pumps are a proven technology. Rather, the issues of concern are the geometrical and operating parameters of the thruster (channel and magnet) that must be realized in order to achieve acceptable overall thruster-ship platform performance and displacement.

A research and development program was, therefore, structured and designed to address the critical technical issues that affect thruster performance. A detailed discussion of the technical issues that were investigated in the program and the rationale to do so are discussed in Ref. [1]. The primary goal of the proposed program was to investigate the steady-state and transient performance of MHD thrusters over broad parametric ranges and to develop validated scaling relationships and models for projecting performance to geometrical and operational parametric ranges of interest for full-scale ships. The program had specific limited objectives; therefore not all technical issues and/or areas of concern such as electrode lifetime, chemical signature, and development of low specific weight magnets were addressed. In the following sections the program pursued is described, specific objectives are defined, the technical approach adopted to achieve the program objectives is outlined, and, the test facility built to carry out the test program is briefly described. The principal focus of this paper, however, is the presentation of the magnetohydrodynamic performance results obtained.

PROGRAM DESCRIPTION

The research program pursued was structured to achieve the following primary objectives: (1) Development of a fundamental understanding of generic MHD related phenomena that can affect the performance of MHD thrusters; (2) Development of a validated analytical capability that can be used to predict the performance of full-scale MHD thrusters over the operational parametric ranges of interest; (3) Generation of a data base relative to the critical MHD loss mechanism that can be utilized to support the design and/or evaluation of MHD thrusters, and (4) Demonstration of the steady-state and transient performance of a large-scale thruster.

The technical approach adopted to achieve these program objectives is as follows.

Technical Approach

The experimental program was structured to focus on and investigate the generic MHD phenomena (loss mechanisms) that can adversely affect MHD thruster performance. The individual tests have been designed to verify predicted changes in thruster performance and, where possible, isolate and quantify individual loss mechanisms. The tests were conducted over sufficiently broad ranges of critical parameters such as magnetic field, geometry, electrical loading, and pressure to develop a broad data base to facilitate development of validated analytical models. The key independent thruster operating parameters investigated were (1) magnetic field, 2 - 6 T; (2) thruster electrical load factor (a measure of current density), 1.5 - 5.0; and (3) pressure, 15 - 50 psi.

The thruster was designed to allow variation of its geometric configuration and was heavily instrumented. The thruster was tested on a unique flow loop that was designed, built, and coupled to the large 6-T magnet (1.0-m-diameter warm bore) at Argonne National Laboratory (ANL) to create a test facility especially suited for investigating MHD thruster performance. The thruster served as the pump for the facility; no auxiliary

mechanical pump was used. The test facility was designed to minimize external-loop type viscous losses that can affect the flow rates generated for specified operating parameters of magnetic field, load factor, etc.; virtually all hydrodynamic losses (>90%) occur within the thruster flow train; the inlet nozzle, MHD channel, and exit diffuser. The concentration of the hydrodynamic losses in the test train facilitates isolation and measurement of the various losses. MHD thrusters with cross-sectional areas of up to 0.2 m^2 can be tested on the Test Facility.

Data Acquisition and Diagnostics

To obtain the data required to quantify the loss mechanisms of interest and performance, both global and local measurements was made. Data derived from global measurements of overall pressure rise, flow rate, applied voltage, electric power input, and magnetic field were used to characterize the performance of the thruster. Local measurements of axial pressure distributions, velocity profiles, voltage distributions, and gas phase distributions, were taken at selected locations to provide the data needed to isolate loss mechanisms, validate the models and help resolve discrepancies between predicted and measured performance.

Velocity profiles were measured immediately downstream of the nozzle to ensure the uniformity of flow entering the thruster, and immediately upstream of the diffuser. The latter measurements were made to reveal the expected differences in velocity profiles along the two directions brought about by Hartmann flattening and end effects.

Pressure distributions along the thruster were measured with high resolution differential pressure transducers. The pressure distribution along the thruster was derived from measurements made at selected axial locations (6 to 9 locations).

A valuable diagnostic tool for MHD flows that was employed was the measurement of voltage distributions over the sidewalls. The voltage profile facilitated isolation of the anode and cathode electrode voltage drops. Voltage profile measurements were focused near the end regions where flow and current nonuniformities are the highest.

Finally, information on the release of gas bubbles released at the electrodes were obtained through view ports by high speed video cameras. A view port was located at the diffuser.

Description of Test Facility and Test Thruster

The facility consists of a simple closed flow-loop that passes through the core of the SCMS-1 magnet. The thruster is centered in the warm bore of the magnet. Equipment is required external to the flow-loop in order to maintain the functions of the magnet, thruster, and test-fluid. A liquid helium refrigerator and liquid nitrogen supply are required for the superconducting magnet. Two major power supplies are required, one to energize the magnet and a 500 kW DC thruster power supply for the thruster. The test-fluid requires external processing equipment for mixing, storing, degassing and temperature control. All control and data-acquisition components are housed in a control room.

The principal technical requirements that set the criteria governing the facility design are (1) achievement of thruster operating parameters as close to prototypic conditions as possible, given the available magnet; (2) control of the loop water chemistry to the extent required for reliable and repeatable test conditions; (3) an operating pressure range of 0-200 psig; and (4) a hydrodynamically uniform and stable inlet flow condition to the thruster.

A more detailed description of the test thruster, facility, and its major components/subsystems is given in Ref. [1].

TEST RESULTS

A prodigious amount of data was obtained from the test program. Data were taken with salt solutions with four different conductivities for the 3 meter test thruster. Tests of the 4 meter thruster were done with salt solutions of two different conductivities and with Instant Ocean.

Each data set (representing an individual test) was subjected to the same detailed data reduction algorithm, which yielded the following outputs: (a) A Run Summary Sheet of all measured and calculated parameters, (b) axial friction factor variation, (c) a bar graph comparing cathode and anode currents, (d) ideal and measured current density by electrode, (e) End Region Wall Voltage Profile, (g) Hartmann Current Profile (upstream and downstream), (h) plots of measured and ideal current densities vs. axial location, (i) ratio of measured and ideal current densities vs. axial location, and (j) axial pressure profile. Approximately 250 data sets have been developed

THRUSTER EFFICIENCY

Efficiency of Three (3) Meter Channel

Thruster efficiencies for the 3 meter channel are presented in Figure 2.0 as a function of the ideal load factor $K = \frac{V_a - V_o}{UaB}$ for the salt solution test fluid with a conductivity of $\sigma = 4.7$ s/m. The ideal load factor is used since the objective is to present the data in a format illustrating the degradation of the ideal efficiency with the individual loss mechanisms. The five efficiency curves shown are those that were derived from the measured data, namely e1, – the ideal electrical efficiency, e2, – the electrical efficiency with end losses, e3 – the actual electrical efficiency (ideal efficiency less electrical losses due to end currents and the non-uniform field distribution), e4 – actual thruster efficiency with no electrical voltage drops and e5 – the actual overall thruster efficiency (which includes all losses). The efficiencies are defined in Table I.

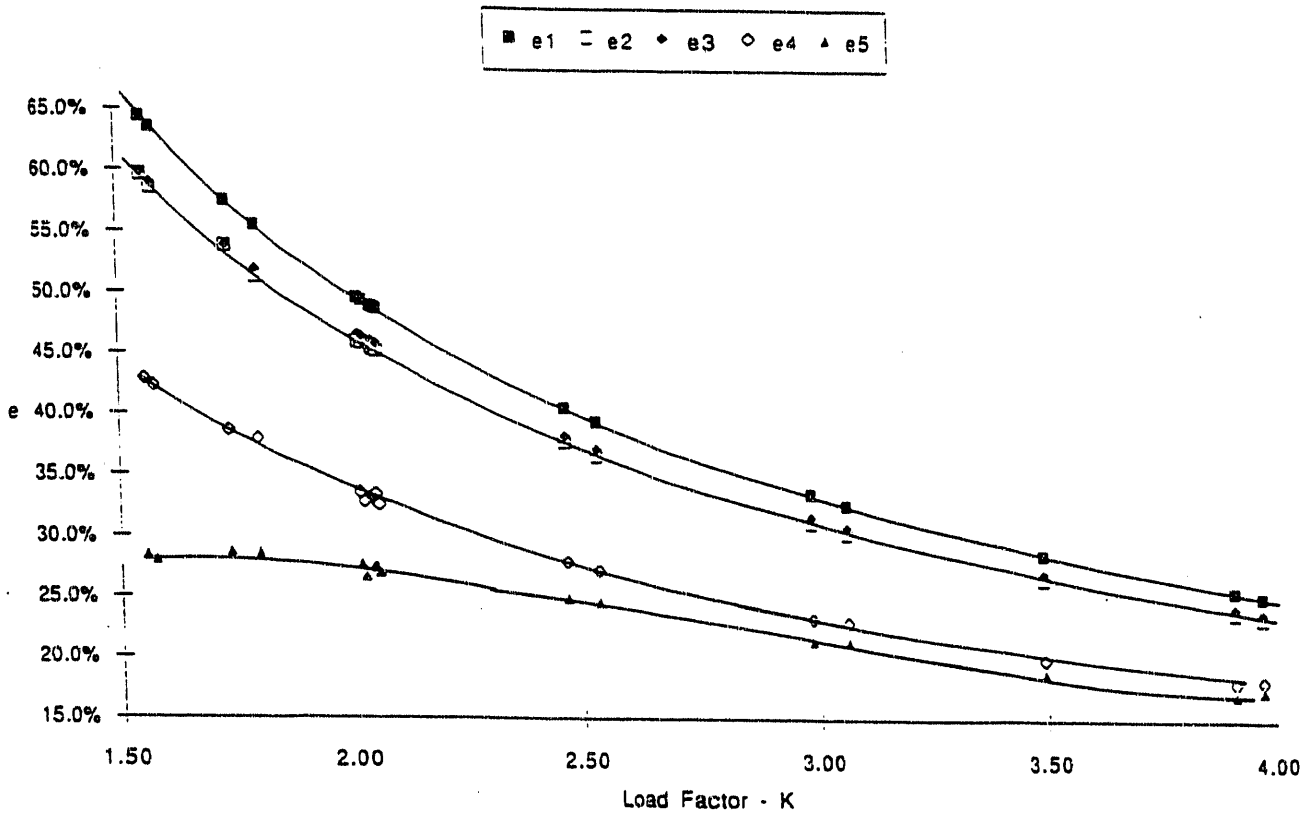

Fig. 2.0. Efficiencies vrs. Load Factor
($\sigma = 4.7$, B = 6T, Run 502 LT 3M)

Table I
Calculation of Efficiencies

$e_1 = \frac{1}{K} = \frac{u\,a\,B}{V_{applied} - V_{over}}$	Ideal Efficiency
$e_2 = \frac{1}{K}\left(1 - \frac{I_{total} - I_{ideal}}{I_{total}}\right)$	Ideal Efficiency Less Endloss
$e_3 = \frac{Q\int J \times B\, dL}{I_{total}\,(V_{applied} - V_{over})}$	Ideal Efficiency Less Endloss and Nonuniformity Loss
$e_4 = \frac{Q\,\Delta P_{thruster}}{I_{total}\,(V_{applied} - V_{over})}$	Overall Efficiency Less Electrode Drop (Overvoltage Loss)
$e_5 = \frac{Q\,\Delta P_{thruster}}{I_{total}\,V_{applied}}$	Actual Overall Efficiency

As expected, the thruster efficiency decreases with increasing load factor. The actual efficiency peaks at ~29% in the lower load factor range ~ 1.5-2.0. It is interesting to note that the electrode drops become the dominant loss controlling efficiency as the load factor decreases. This is due to the fact that as the load factor is decreased the applied voltage decreases, making the electrode drop (which is relatively constant) proportionally a larger fraction of the applied voltage. Conversely, as the load factor increases the importance of the electrode drop diminishes as the applied voltage increases. The frictional loss impact on thruster performance increases as the load factor is increased, becoming the dominant loss, allowing for the normal decrease in electrical efficiency. Finally, it should be noted that there is little effect of field nonuniformity on the electrical efficiency as expected in the load factor ranges studied, since the variation in field over the 3 meter length is relatively small except for ¼ meter sections at the entrance and exit of the thruster where it begins to drop off relatively rapidly, see Fig. 3.0.

Effect of Fluid Conductivity on Efficiency The thruster efficiency was investigated as a function of salt solution test fluids of increasing conductivity (σ = 8.9, 13.2, and 16.2 s/m); the results for the fluid with a conductivity of 13.2 s/m is presented in Figure 4.0. As is evident, the trends are essentially similar to those described above for the test fluid with σ = 4.7 s/m. The major impact of increasing electrical conductivity is to increase velocity for a specified load factor. This in turn results in increased pressure losses which adversely impact overall efficiency. However, with increased velocity the applied voltage is higher and the relative effect of the electrode drop is diminished. Therefore, the overall impact is the net result of these two competing affects; the impact can be positive or negative. A comparison of the efficiency curves (Figures 3.0 and 4.0) indicates that the impact tends to be positive. For example, in the load factor range of 1.6 to 1.8, a peak overall efficiency of ~36% is reached, which is significantly higher than that achieved with the lower conductivity fluid.

It is important to note that these trends and impacts will vary with thruster size since the relative magnitude of the individual losses will vary. As thruster size (distance between electrodes) increase the relative effect of electrode drop will diminish; likewise the pressure drop will diminish.

Efficiency of the Four (4) Meter Thruster Channel

The efficiency of the four meter thruster channel tested with a salt solution of σ = 5.1 s/m is shown in Figure 5.0. Several significant differences in trends and impacts relative to the three meter channel is evident. The principle difference is the substantive electrical loss associated with the field nonuniformity - the difference between e2 and e3. The additional meter of electrodes added to the three meter channel lie within regions where the field is dropping off very rapidly in this region the local load factor is quite high relative to the central region, thus introducing greater ohmic losses. A second evident difference is that the electrode voltage drop is significantly less and has less of an impact on the efficiency. The measured electrode drops were substantially less than measured on the three meter channel, as discussed in a later section.

An issue relative to presentation of the efficiency data for the four meter channel is the definition of a load factor. It was concluded that since the objective was to isolate losses relative to the ideal channel, the most appropriate definition would be to define the load factor as

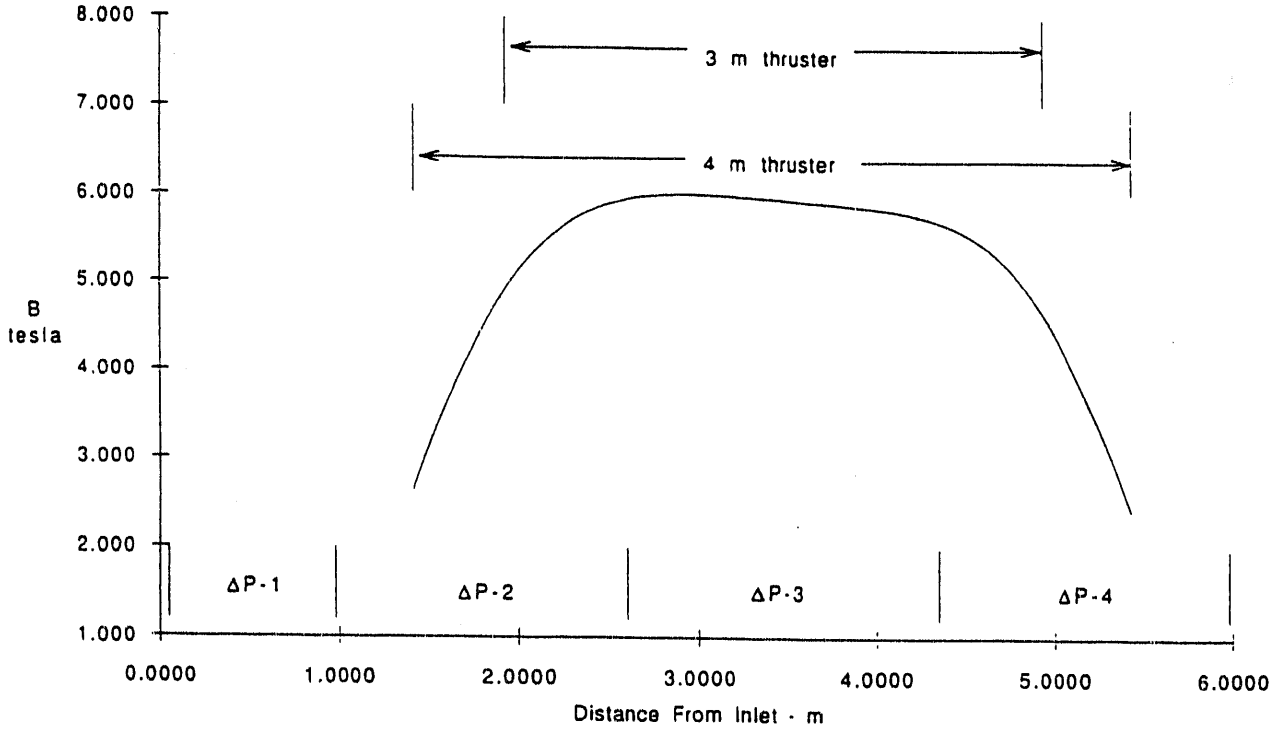

Fig. 3.0. Position of Field Relative to Pressure Taps and Electrodes

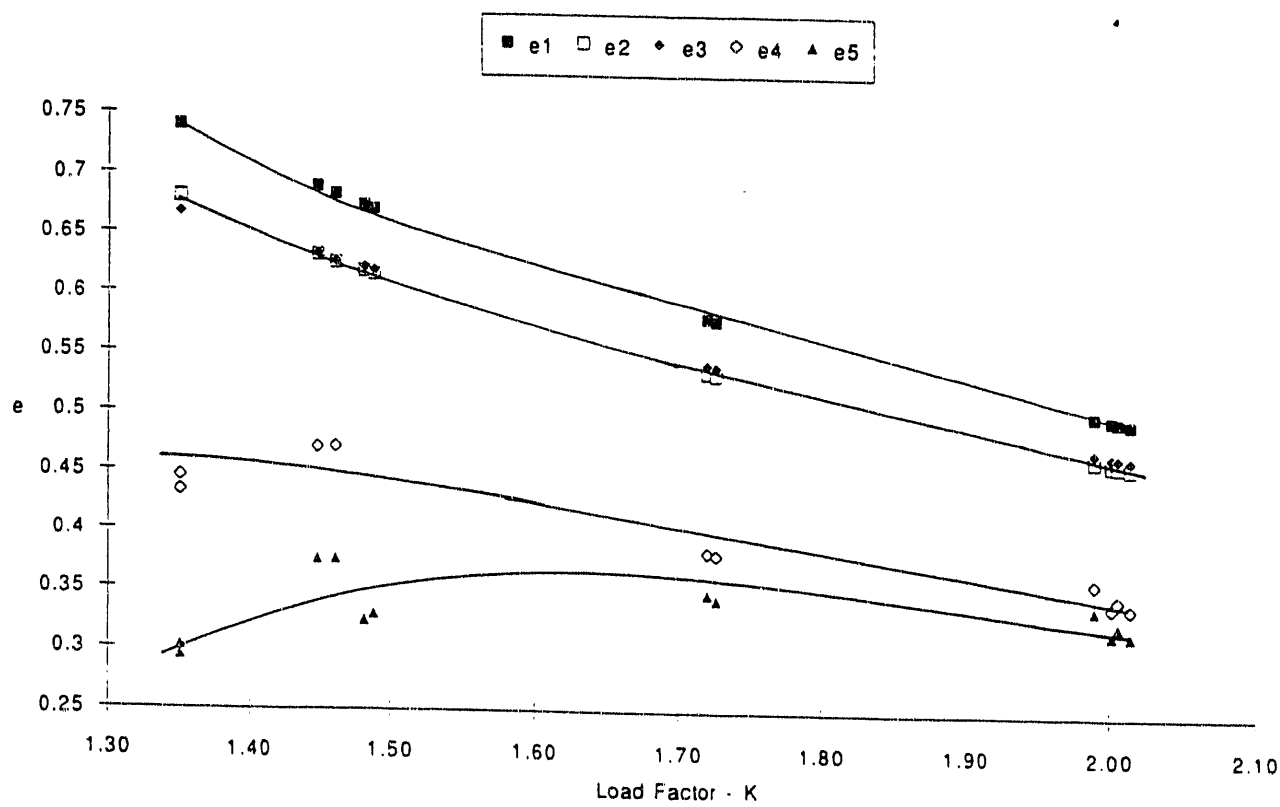

Figure 4.0. Efficiencies vrs. Load Factor
(σ = 13.2, B = 6T, Run 603, L_T = 3M

$$K_{i,4} = \frac{V_a - V_o}{Ua\overline{B}}$$

where $\overline{B}$ is the average field over the central three meter length and V_o is the voltage drop in the center of the channel. Comparisons between the three meter and four meter channels are facilitated with this definition as well.

The efficiency of the four meter channel as expected is less than that of the three meter channel, see Figures. 3.0 and 5.0. The drop off in efficiency is due essentially to the effect of the field nonuniformity, as discussed above; the channel is operating at effectively larger load factors (resulting in greater ohmic losses)..

The efficiency of the four meter channel operating on a test fluid made from Instant Ocean was essentially the same as that shown for the four meter channel operating with the salt solution with the same equivalent conductivity, see Figure 5.0.

Comparison of Data With 3-D Code The measured mechanical efficiency (e2) and electrical efficiency (e3) were compared with a 3-D thruster code that was developed from the ANL 3-D plasma channel code. The code solves for the three-dimensional fluid flow velocity distribution and current distribution within the thruster, as well as in the inlet and outlet end regions. Since the code does not solve for the overvoltage, the measured value obtained from the voltage profile in the center of the channel was inpacted. The code thus solves for the overall efficiency when no overvoltage is present. The electrical solution generated is equivalent to e3.

A comparison of measured and predicted values of the efficiencies are given in Fig. 6 for a salt solution of $\sigma = 4.7$ s/m. As is evident, the comparison between theory and data is excellent. Similar good comparisons were obtained with the higher conductivity fluids as well.

LOSS MECHANISMS

Electrical Voltage Drops (Overpotential)

There are a number of factors that impact the near electrode voltage drop. Several of the most important are the variation of the test fluid chemistry with time due to closed loop operation, the nonuniform axial local current densities and the variation in boundary layer parameters with changing operating conditions. The data obtained reflects and underscores the complexity of the problem. Great pains were taken to attempt to develop reliable and repeatable voltage drop data, because of the impact of the measured electrode drop on all data analyses and interpretation (see Table I). Because of its critical nature, it is appropriate to review how the electrode drops were developed from the voltage profiles that were measured between electrode, as well as the underlying assumption.

Typical voltage profile data are shown in Figure 7.0 taken on the four meter channel being tested with a salt (NaCl) solution. As expected, the central portion of the profile (usually 6 voltage taps) exhibit a linear relationship. A straight line was fit to this point with a least square algorithm. The linear relationship was then extrapolated to the anode and cathode walls to establish a voltage drop on each surface, as indicated. The underlying assumption for this procedure is that the equal potential lines between the electrodes are straight; therefore, the voltage measurement made on the B walls accurately reflect the

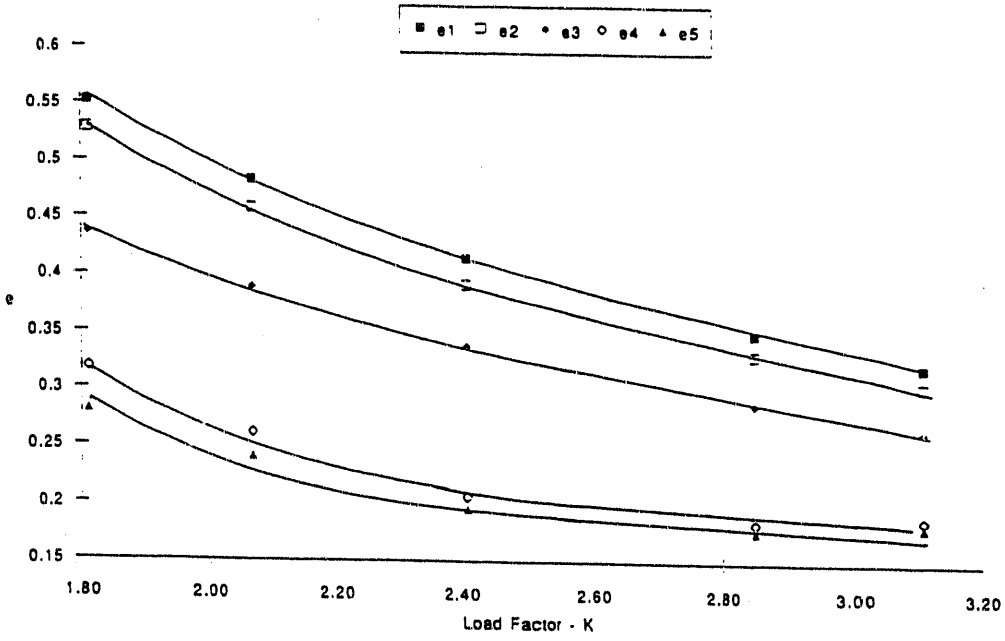

Fig. 5.0. Efficiencies vrs. Load Factor,
(σ = 5.1, B = 6T, Run 902, L_T = 4M)

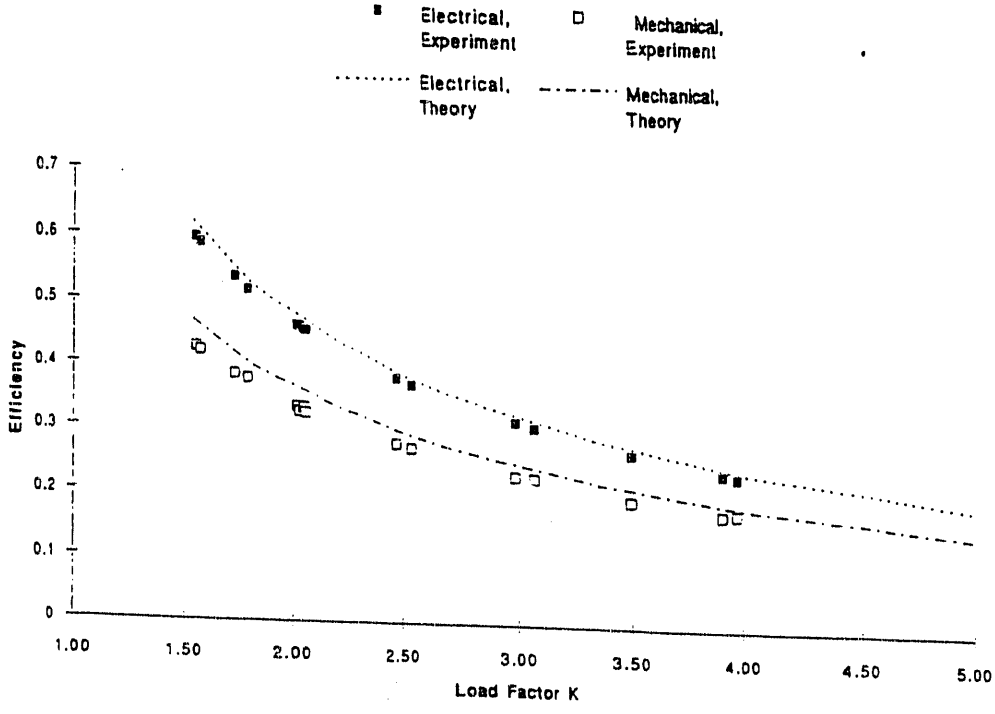

Figure 6.0. Comparison of Experimental and Predicted Efficiencies
(B = 6T, L = 3M, σ = 4.7 s/m)

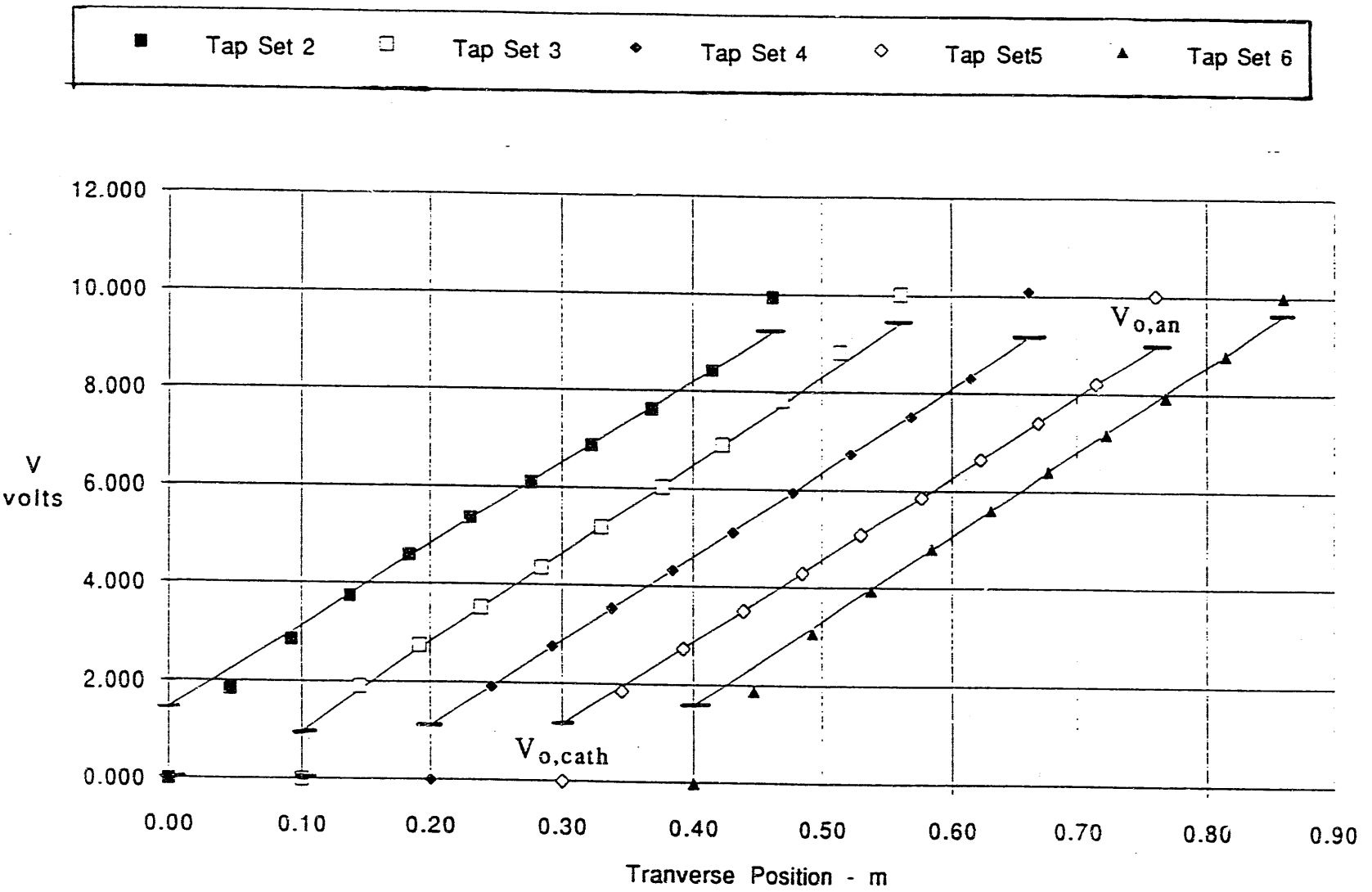

Fig. 7.0. Typical Wall Voltage Profiles

voltage gradient at any point between the B walls. The second inherent assumption is that there are no voltage drops on the surface of the voltage taps since no current flows through the taps. A final assumption is that there is no significant collection of gas bubbles on the B wall surfaces that would impact the voltage profile.

The Three Meter Channel Electrode Voltage Drops The electrode voltage drops were measured for the four different fluid conductivity salt solution test fluids (4.5 s/m, 8.9 s/m, 13.2 s/m and 16 s/m): data are presented for fluids with σ = 4.5 and 16 s/m in Figures 8.0 and 9.0. As is apparent Tafel type kinetic behavior (a linear relationship on a plot of overvoltage vs. ln current density) is observed in the data. As can be seen for the fluid of conductivity of 4.5 (Figure 8.0) the overpotential consists of a thermodynamic (reversible) component and a kinetic (irreversible) component. For this conductivity the so-called thermodynamic potential is roughly constant up to a cathodic and anodic current density of about 150 A/m^2. This exchange current is consistent with that found from the Tafel plots for the Eltec DSA electrode used in the thruster (i_o = 130 A/m^2) thus reinforcing the supposition of a preferential chlorine evolution at the anode. Tafel kinetic behavior is also observed for the fluid with σ = 16 s/m, Figure 9.0; however, the thermodynamic component is not readily ascertainable and the overvoltage seems to start increasing at a lower current exchange, indicating that different reaction mechanisms are occurring. It can also be noted that the Tafel slope (in the kinetic regime) decreases as the conductivity increases, indicating that for a given current density, lower overvoltages are expected with higher conductivity solutions. Lower thermodynamic potentials also occur with higher conductivity fluid, which is consistent with the Nernst Equation. It is, however, important to note that the Tafel slopes measured for a flowing fluid are larger than those recorded when the fluid is at rest. The reason is believed to lie in the hydrodynamic boundary layer resistance enhancement of the overvoltage that is not present in Tafel plots established for motionless fluids.

For the 3-m-electrode test with NaCl solutions, it was found that the total overpotential (anode+cathode) varies along the axial length of the thruster electrodes in a manner as indicated in Figure 10.0 which is typical of the data obtained. In this Figure, the overpotential is plotted at three axial positions, upstream near the entrance of the channel (1), middle (2), downstream near the exit of the channel (3). As can be seen, at low current densities, the overvoltage is about 2.6 volts and increases as the average current density increases. As is evident, the voltage drop is the highest at the ends of the thruster electrodes because the electrode current density in these areas is larger due to the existence of the end currents, as discussed in the following section. It should be noted that in all cases the measured center value of the electrode drop was used for subsequent analysis of each run, e.g. for deriving end losses, load factors, etc.; the rationale for this decision is presented in the subsequent sections.

The Four Meter Channel Electrode Voltage Drop A more involved overvoltage pattern was observed for the four meter channel, as can be seen in Figures 11.0 to 13.0, where cathode, anode and total electrode drops are shown as a function channel length for a salt (NaCl) solution test fluid. Again, these data are typical of that obtained in the tests. As can be seen in Figure 11.0, the cathodic overpotential measured at the center of the channel at low current (characteristic of the thermodynamic range) is significantly lower than that measured in the three meter channel in a similar current density; from an average value of 0.75 volts to a value of 0.2-0.4 volts. At the anode side (Figure 12.0) the overpotential is also reduced, from 1.3 V typically found in the 3 meter channel to 0.8 V. Such changes in

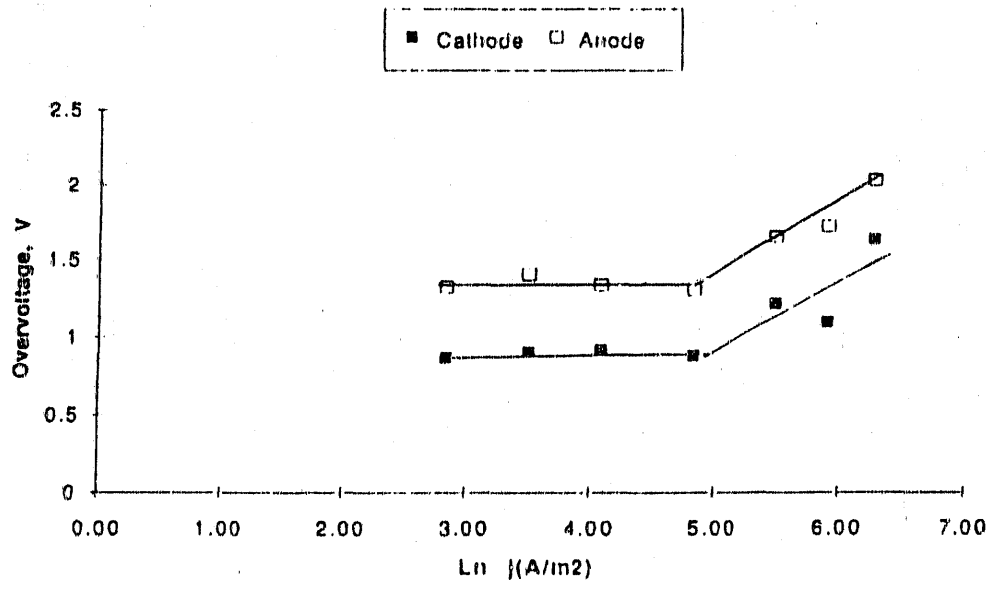

Figure 8.0. Tafel Plots of Overvoltage vrs. Current Density
(σ = 4.6 x/m, L = 3M, Salt Solution)

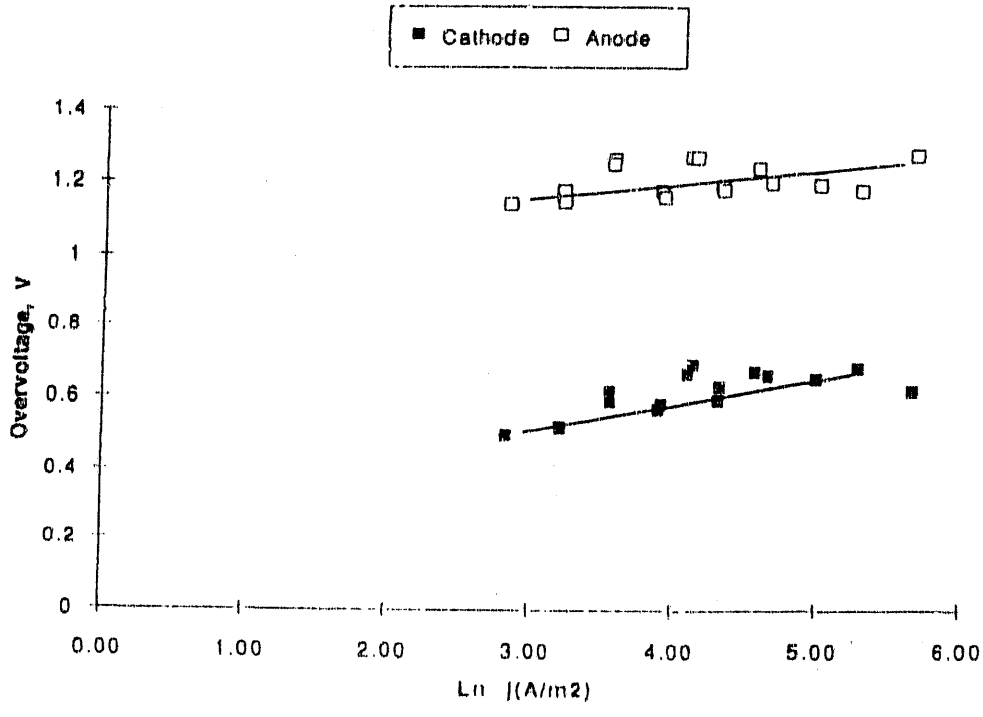

Figure 9.0. Tafel Plots of Overvoltage vrs Current Density
(σ = 16.0 s/m, L = 3M, Salt Solution)

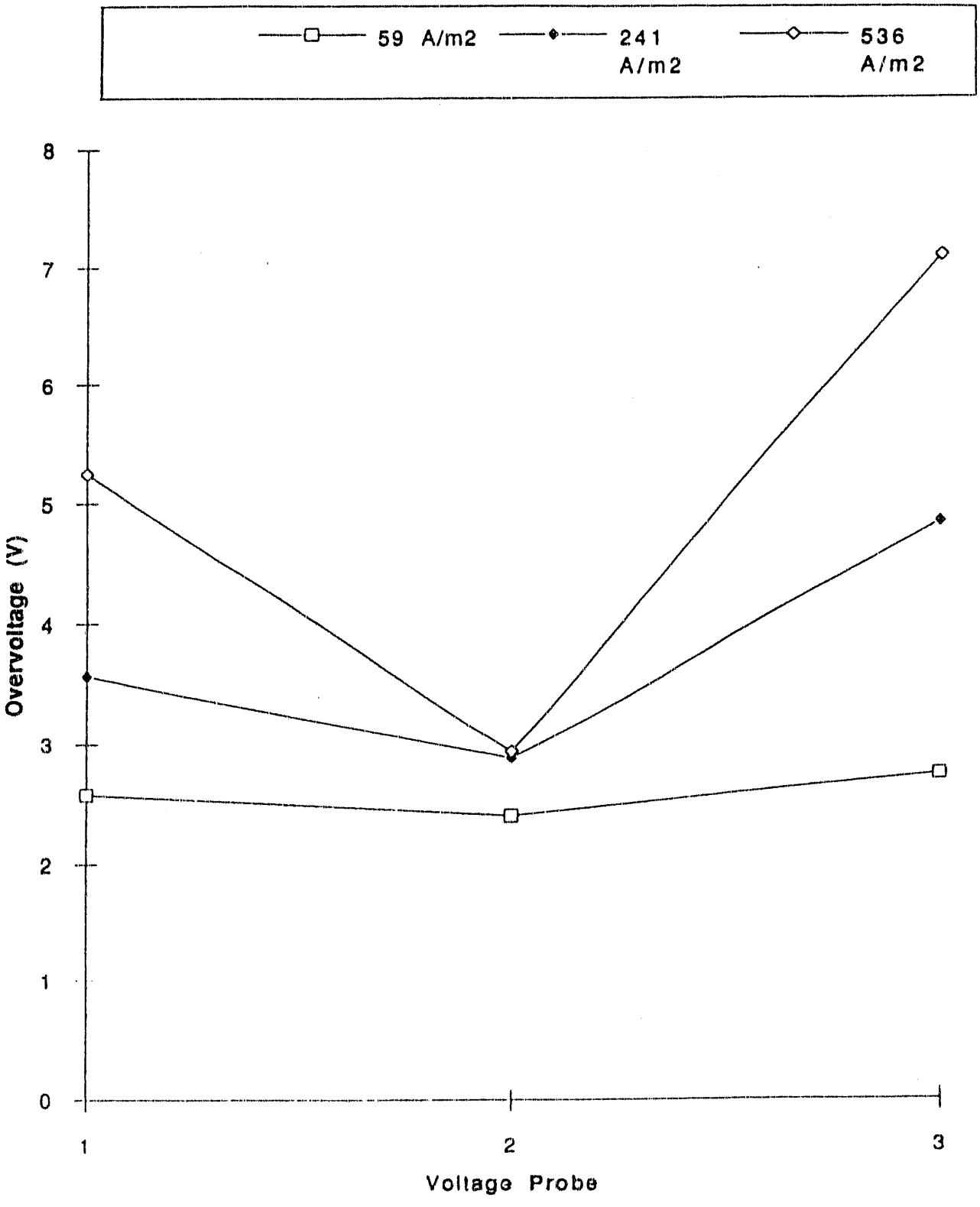

Figure 10.0. Experimental Global Overvoltages Along Channel
(σ = 4.6 s/m, L = 3M, Salt Solution)

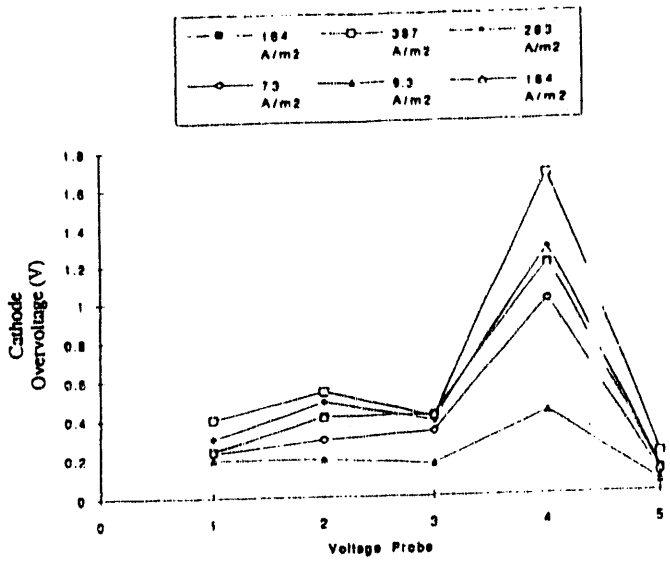

Figure 11.0. Cathode Overvoltage Measured at Five Locations (End Upstream (1-2), Middle (3) and End Downstream (4-5)) Along the Thruster at Several Average Current Densities (4M Electrode Length, $\sigma = 4.6$ s/m, NaCl)

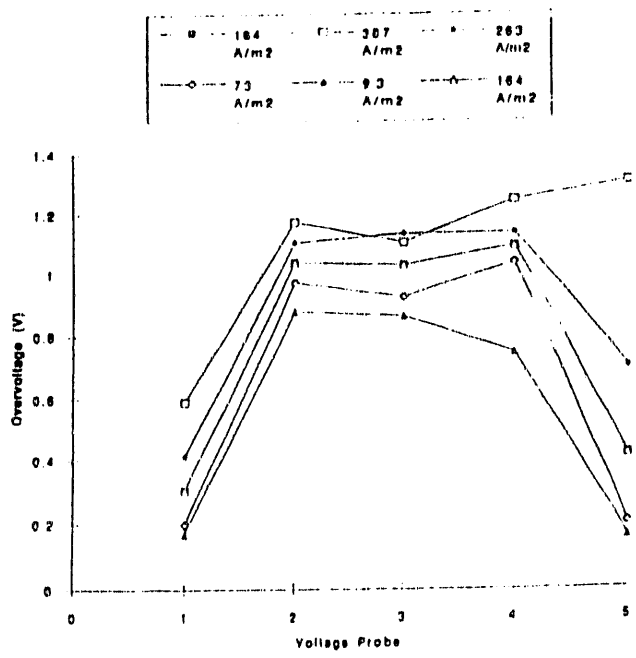

Figure 12.0 Anode Overvoltage Measured at Five Locations (End Upstream (1-2), Middle (3) and End Downstream (4-5)) Along the Thruster at Several Average Current Densities (4M Electrode Length, $\sigma = 4.6$ s/m, NaCl)

overpotential may indicate the presence of other chemical species impacting the conventional formation reactions of hydrogen and chlorine.

Midway through the test program (at the completion of the three meter performance tests) it was determined that the test fluid was being contaminated with a significant quantity of iron and/or iron compounds that apparently evolved from the periodic transfer of test fluid between the storage tank and test facility. Because of limited time and resources, no new test fluids were prepared for the four meter channel; the original batch of test fluid used in the three meter channel test was altered as required to achieve the desired conductivity for the four meter channel tests. It appears, therefore, that higher quantities of iron compound were present in the test fluid (relative to the tests conducted on the three meter channel). This fact suggests that the following chemical reactions could have occurred at the cathode and anode.

Cathode $Fe^{++} + e^{-} \rightarrow Fe \quad E_o = -0.44V$

Anode $Fe^{++} \rightarrow Fe^{+++} + e^{-} \quad E_o = 0.77V$

These reactions would yield a total overpotential of about 1.2 volts; this value is very close to what was measured (see Figure 13.0, at low current densities. The drastic drop of overpotential at the anode at the entrance and exit of the thruster ,probes 1 and 5 is puzzling, because an increase in overpotential would normally have been expected since the current density is maximum at these locations (Tafel kinetics).

Electrode voltage drops measured during performance tests of the four meter channel with Instant Ocean are presented in Figure 14.0. Shown are the axial measured electrode drops. As is evident, no clear trends in the total overvoltage behavior is discernible in regard to current density, and variation along the axial length, etc. The same type of anomalies seen in the salt solution test fluids (Figures 11.0 to 13.0) are evident. The observed behavior suggests that other factors that are varying along the channel length may be impacting the overvoltage measured on the B wall, such as changes in ion species concentration, during closed loop operation, variation in distribution of gaseous bubble volumetric fractions, competing channel reactions, etc. It should be noted that the Instant Ocean test fluid was prepared from a new batch of deionized water and had relatively little operating time (ampere hours). The anomalous behavior of the electrode drop (overvoltage) recorded in the tests conducted on the four meter channel require much more detailed scrutiny and an evaluation. Currently, the trends noted are inexplicable.

Electrical End Losses

The end losses in the thruster were determined via a comparative evaluation of the measured current distribution with the calculated current distribution of an ideal thruster. The difference is attributed to the end currents. The end currents are thus sensitive to the accuracy of the measured values of velocity, electrode voltage drop, electrical conductivity and field distribution. An indication of the accuracy of the computed ideal currents can be obtained by plotting the ratio of the measured electrode current to the computed ideal current as a function of axial length, as shown in Figure 15.0; this plot is typical of the hundreds analyzed. The central portion of the channel contributes no current to the end region; therefore, the ratio of the measured and computed currents should be unity; such a condition is indicated for the data shown in Figure 15.0. Furthermore, as expected, the measured current is greater than the computed ideal current on the entering and exit

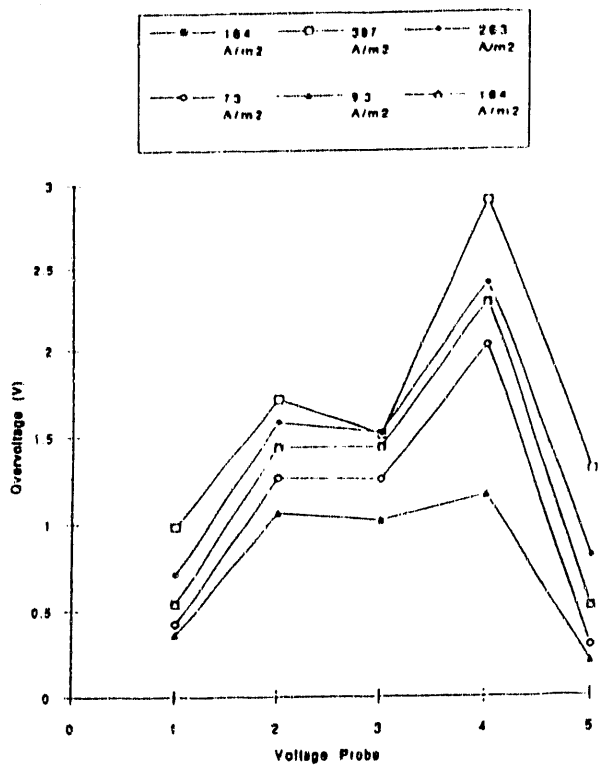

Figure 13.0. Total (Anode + Cathode) Overvoltage Measured at Five Locations (End Upstream (1-2), Middle (3) and End Downstream (4-5)) Along the Thruster at Several Average Current Densities (4M Electrode Length, σ = 4.6 s/m, NaCl)

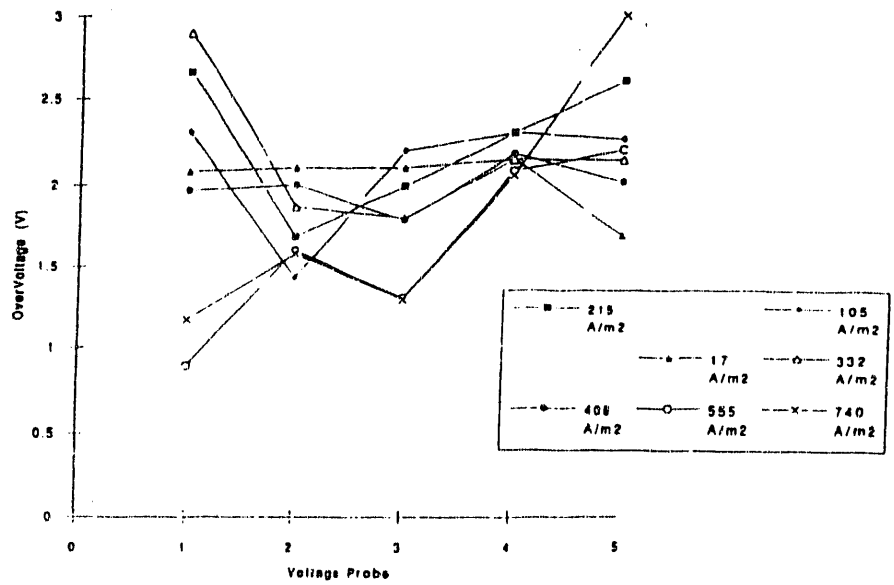

Figure 14.0 Total (Cathode + Anode) Overvoltage Measured at Five Locations (End Upstream (1-2), Middle (3) and End Downstream (4-5)) Along the Thruster at Several Average Current Densities (4M Electrode, Length) σ = 4.6 s/m, Instant Ocean)

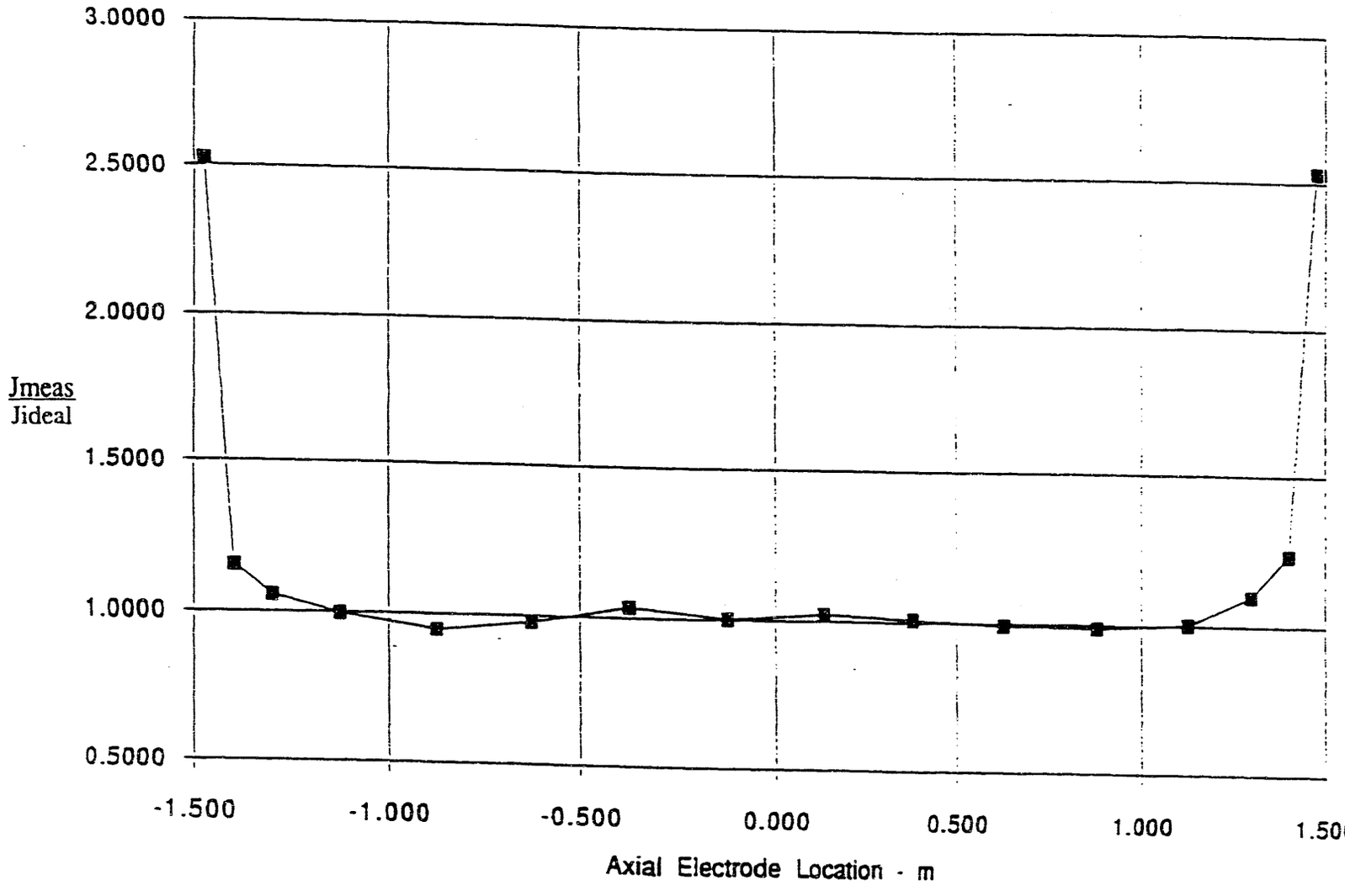

Figure 15.0 Jmeas./Jideal vrs. Axial Location
(B = 6.0T, K = 2.46, U = 3 M/sec, L = 3M)

electrodes. The currents flowing in the end region essentially emanate from these electrodes; this fact is confirmed by the 3-D analysis.

End Losses in the Three Meter Channel The end losses for the three meter channel derived from tests with salt fluids of σ = 4.6, 8.9, 13.2, and 16.2 s/m are given in Figures 16.0. The end losses are presented as the fraction (percentage) of the total thruster current which pass through the end region (external to the thruster electrode region) as a function of load factor. As is evident, the electrical end loss increases as the load factor is reduced. This trend is consistent with theory and analysis; shown on Figure 16.0 is the theoretical prediction of the end loss obtained from the 3-D computer simulation. The trend is accurate, but the theoretical prediction is ~10% higher than the data. This discrepancy is believed to be due to the fact that no allowance was made in the analysis for a higher overvoltage on the end electrode from which the end current flows, see Figure 15.0. The predicted imposition of a higher overvoltage would reduce the predicted end loss.

The end current loss factor exhibits little or no dependency on fluid conductivity for a specified load factor. In a similar vein, there appears to be no effect of magnetic field. This is consistent with theoretical considerations. It should be noted, however, that the higher conductivity fluids operated at lower load factors and thus tended to have higher end losses.

End Losses in the Four Meter Channel The extraction of definitive end current loss factors from the four meter channel tested with both salt solutions and Instant Ocean is proving to be difficult at best, because of the inconsistencies in the measured electrode voltage drops (overvoltage). As discussed, the electrode drops exhibited unusual and unexplained behavior and directly impact the calculation of the end currents. The basic problem encountered is illustrated in Figure 17.0, which shows a typical plot of the ratio of the measured current to the ideal current as a function of axial length for the four meter channel. As can be seen, the ratio is less than one on the entrance and exit electrode sections of the thruster, furthermore the ratio tends to fluctuate about unity more so than observed in the three meter channel. The net result of such a pattern is that the end currents calculated from the difference of the total measured and ideal currents are less than they should be, thus reducing the end loss factor. The deviations in increase as the load factor is reduced. The measured voltage drop in the center of the thruster was used in the calculation of the ideal currents as was done in the three meter channel. Because the voltage drops are inexplicably low the calculated ideal currents tend to be on the high side, thus decreasing Jm/Jideal.

A typical plot of the end loss factor as a function of load factor is given in Figure 18.0 for an σ = 5.1 solution. Shown on the figure are two curves. The bottom curve is based on the calculation of the end loss utilizing the measured values of the overvoltage in the center of the thruster; the upper curve is based on assumption of a constant electrode drop of 2.2 volts (the thermodynamic overpotential). As is evident, the impact on the trend of the data is dramatic. In the higher load factor range the end loss factor drops off with increasing load factor similar to the three meter channel. Below a load factor of ~2.4 the curves based on the measured electrode drop indicates that the end loss factor decreases with decreasing load factor. This is believed to be an inaccurate result, since it is inconsistent with theory and the three meter results. The trend exhibited by upper curves of end loss based upon the assumed constant value of overvoltage are consistent with theory, namely that the end loss increases as the load factor decreases and the three meter channel data.

Comparison of Experimental and Predicted End Currents Versus Load Factor (B=2.6T, L=3M, Salt)

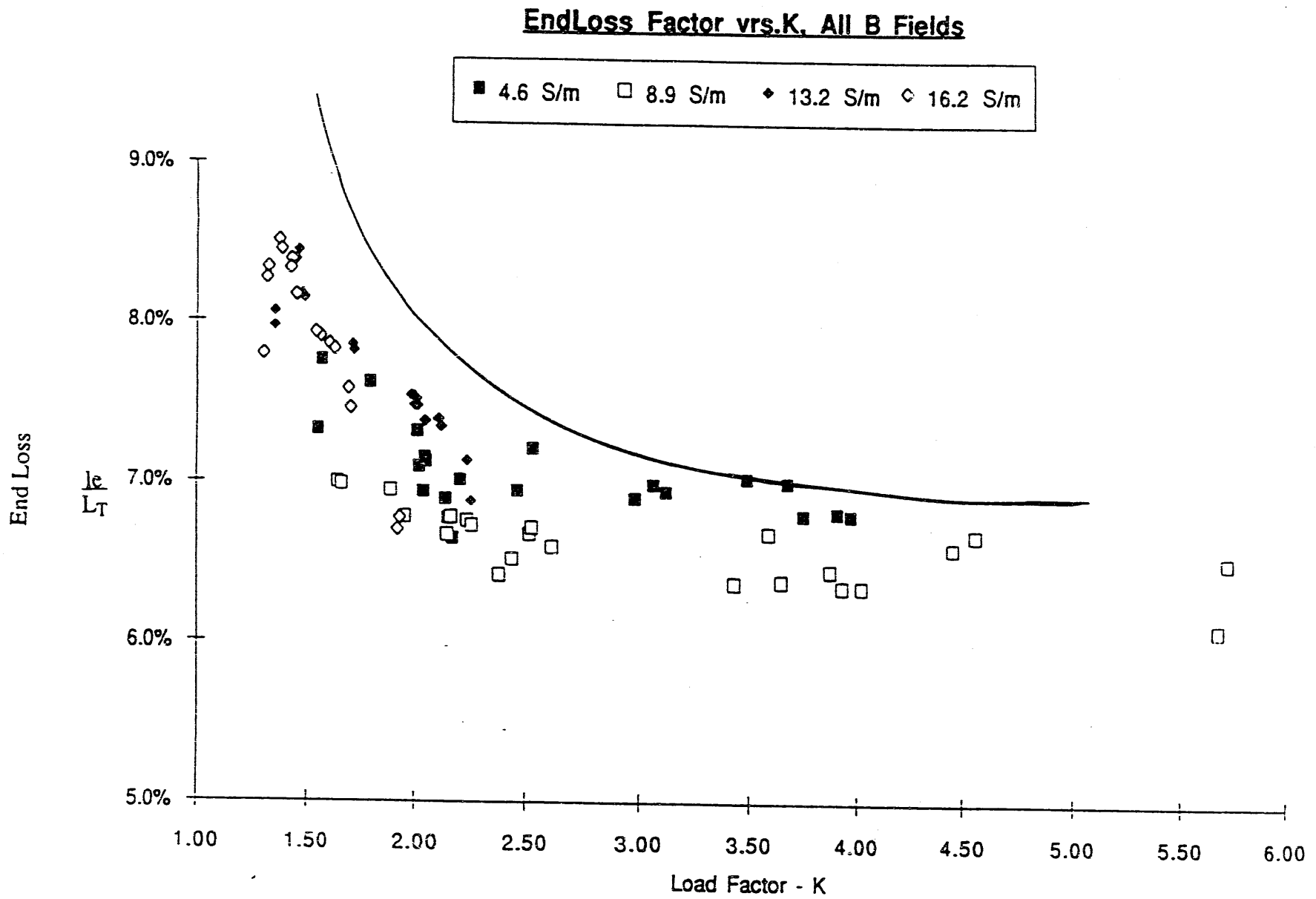

Figure 16.0 Comparison of Experimental and Predicted End Currents Versus Load Factor (B = 2.6T, L = 3M, Salt Solution)

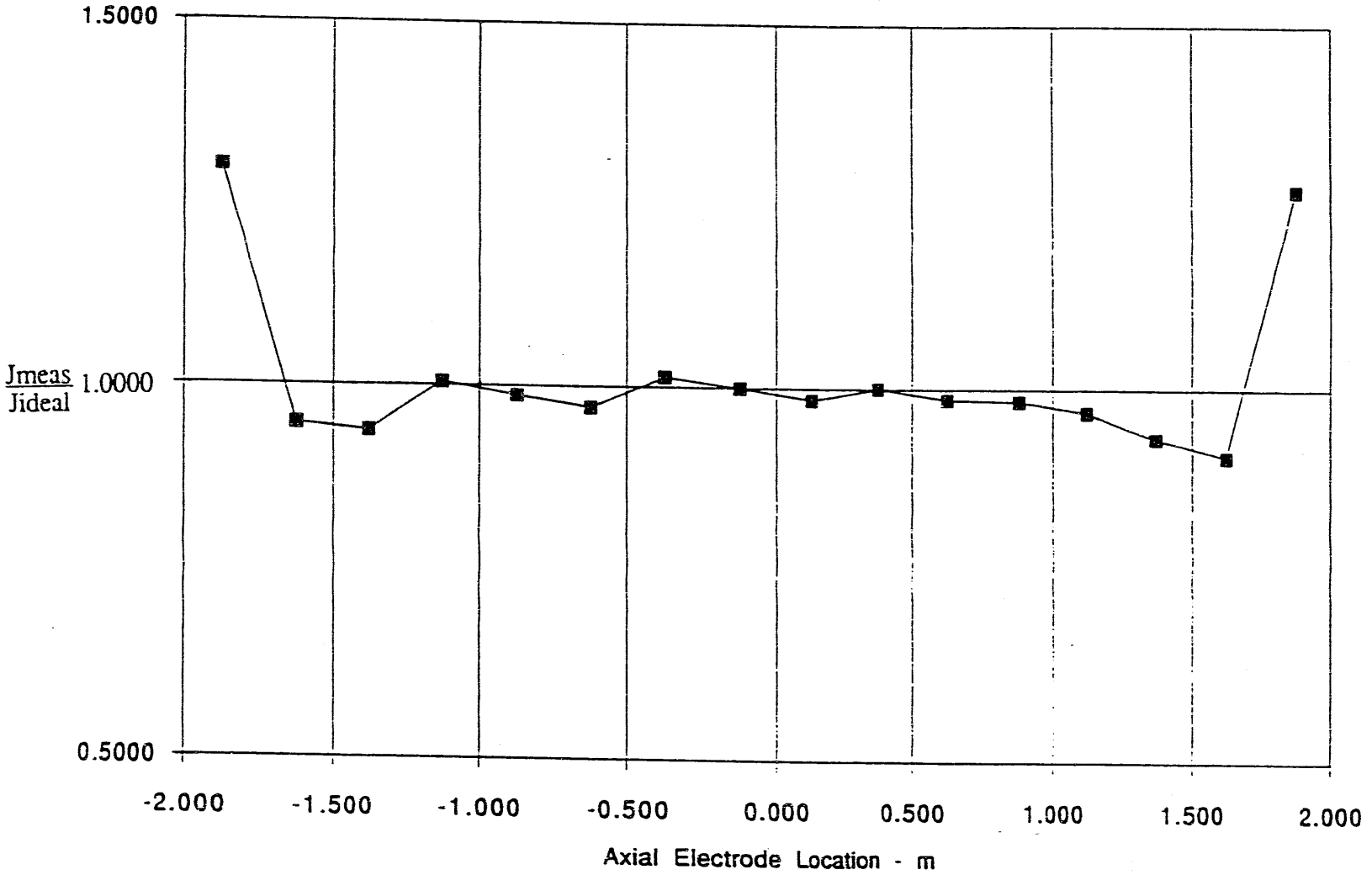

Figure 17.0. Jmeas./Jideal vrs. Axial Location
($B = 5.4T$, $K = 1.81$, $\sigma = 5.1$ s/m, $L_T = 4M$)

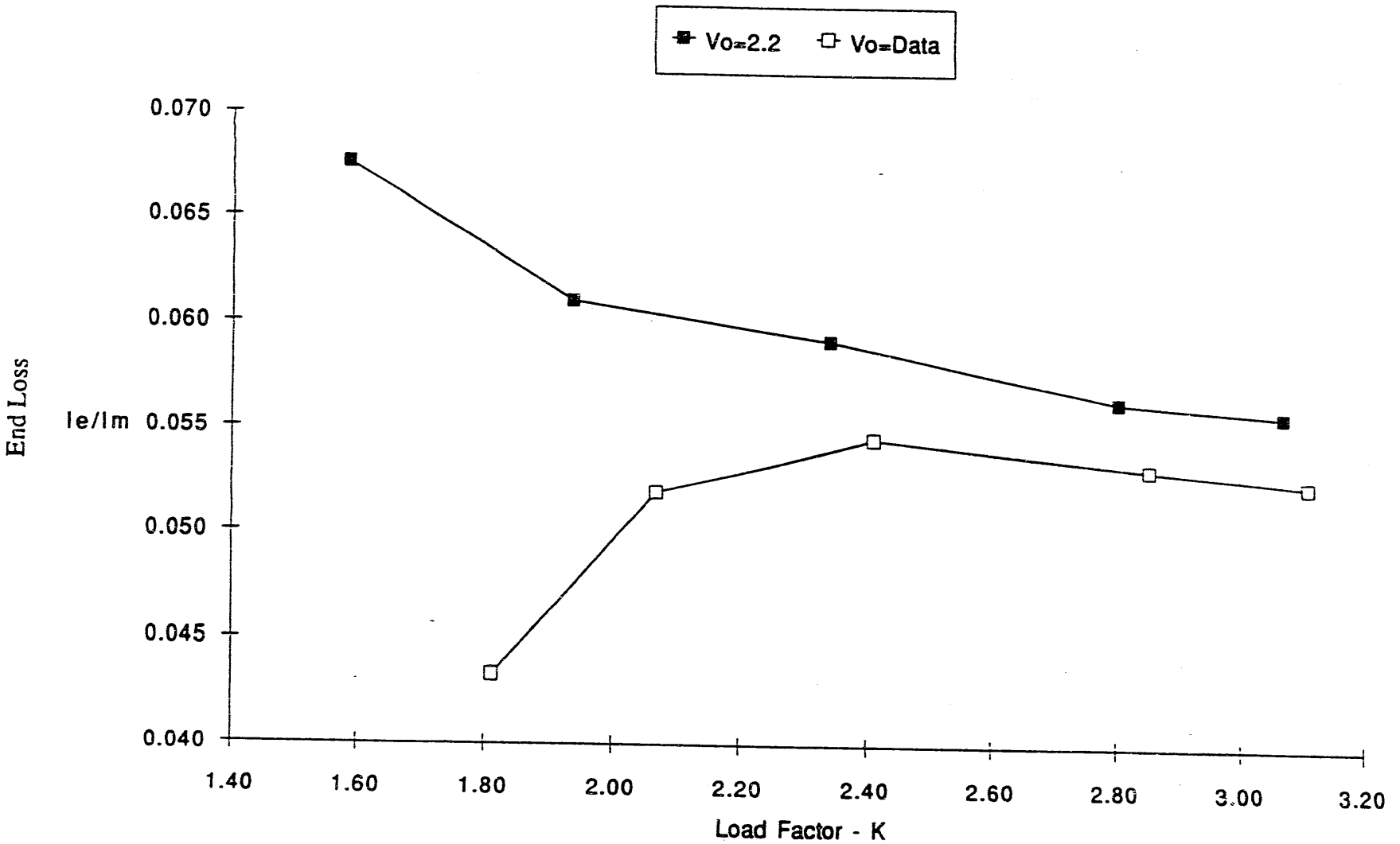

Figure 18.0 Ie/Im vrs. K, B = 6T, σ = 5.1, Run 902, L_T = 4M

The magnitude of the end loss for the four meter channel for a specified load factor is lower than measured for the three meter channel. This is as expected, since the four meter channel has a higher aspect ratio.

The end losses derived from tests of the four meter channel with the test fluid made from Instant Ocean are similar to those cited above.

VISCOUS (FRICTIONAL) LOSSES

Friction coefficients were extracted from the extensive pressure drop axial profile data taken on the thruster. It was recognized that the viscous losses (friction coefficients) would be impacted by a number of factors, e.g. entrance velocity profile evolution of the gaseous species on the electrode surfaces, the magnetic field which alters the velocity profiles on the B wall, and end currents which alter the velocity profile on the electrode wall, etc. Because of such impacts, the flow through the channel does not reach fully developed conditions. The frictional coefficients, therefore, are examined for trends vis a vis Reynolds and Hartmann numbers and compared with fully developed flow coefficients, which are generally used in preliminary design and evaluation studies.

Before presenting the pressure drop data, it is appropriate to review the position of the pressure drop measurements, relative to the principal active field distribution, see Figure 3.0. The axial center of the thruster is at the three meter distance. As is apparent, pressure drop measurements ΔP-2 and ΔP-4 are over a length which have steep magnetic field gradients; also the field in these segments approaches zero and then reverses direction at about ¼ meter from inlet and outlet; the magnitude of the reverse direction field is below 0.2 T. Fringe electrical currents also exist in the lengths, especially for the four meter thruster. The principal magnetic field-flow interactions occurs over the length where ΔP-3 is measured; in contrast to the segments where ΔP-2 and ΔP-4 are measured the central portion of the thruster over which the ΔP-3 measurement is made has a relatively uniform field with a taper of ~.15 T/meter. In all the segments Hartmann layer effects evolve on the B wall; also bubble formation on the electrodes is occuring. The central portion of the channel over which the ΔP-3 measurement is made can be expected to be dominated by Hartmann layer development on the B wall and the effects of gaseous bubble evolution from the electrode surfaces which can counteract each other.

Still another important factor impacting the viscous loss (friction coefficient) is the fact that the velocity profile entering the thruster is essentially flat. This was confirmed by pitot tube traverses, therefore, developing flow is immediately encountered (even before the field region) and is characterized by substantially higher coefficients.

It is important to note that the manner in which the data was acquired resulted in the following characteristic responses of the thruster. For a fluid of specified conductivity, the ratio of the Ha/Re decreased as the load factor, K, increased (due to increase in velocity); also the gaseous bubble evolution increased as K increased and hence Ha/Re decreased. As the fluid conductivity increased the Hartmann number increased; also the current density and Reynolds number increased, relative to lower conductivity fluids for a specified load factor. These changes need to be borne in mind as the data is reviewed.

The Three Meter Channel Typical data showing the variation of the frictional coefficients derived from measured pressure drops relative to the computed fully developed frictional coefficients (at the same Reynolds number with L=0, J=0) as a function of Ha/Re

is given in Figures 19.0 to 20.0; for the test fluid with $\sigma = 4.7$ s//m. Interesting trends are discernible in each segment of the channel.

In the axial segment ΔP-2 (Figure 19.0,) as can be seen, the friction factor ratio is substantially above unity and appears to exhibit a slight peak before dropping off as the velocity and Reynolds number decreases. Perhaps the most interesting trend is observed in the ΔP-3 segment, the central portion of the thruster, see Figure 20.0. The average friction coefficient in the segment tends to be 20% below the fully developed flow coefficient at low ratios of Ha/Re (high velocity and Reynolds number) and then to gradually increase as

the Ha/Re ratio increases (thruster velocity and current density decreases), reaching unity at about Ha/Re=3.5×10^{-4}. It appears that the gaseous bubble evolution on the electrode surface may be the dominant mechanism that reduces the friction. As the current density and bubble generation rate drops (higher Ha/Re ratios) and the Hartmann number layers developed on the B-wall the friction coefficient increases.

In the final segment of the thruster ΔP-4 as shown on Figure 21.0 the friction coefficient again is above the fully developed flow value; the value tends to level off and/or peak at a value 20% higher than fully developed flow at a Ha/Re of 2.5×10^4. The increase noted may be attributable to the competing influence of the drop off of the bubble generation rate and magnetic field effects on the velocity on the B-walls (Hartmann effect).

The substantial variation of the friction factor from segment to segment in the thruster is clearly shown in Figure 22.0 which presents the friction factors for segments ΔP-2, ΔP-3 and ΔP-4 as a function of Ha/Re. As can be seen the highest friction coefficients are in the ΔP-2 segment with the lowest values in the center of the channel ΔP-3. The coefficients in the ΔP-4 segment are intermediate to them

In general, trends similar in some respect, but substantially different in others, were observed in the friction factors derived from tests of the fluids of higher conductivity. Analyses of these data are not complete as yet.

<u>Four Meter Channel Frictional Coefficients</u> Analyses of the frictional coefficients derived from the 4 meter data have not been completed as yet. Similar substantive variations in frictional coefficients as observed in three meter channel are being seen. The magnitude and trends of the frictional coefficients, however, are significantly different. As an example, a particularly substantive difference is observed in the ΔP-3 segment. In the three meter channel, as shown in Figure 20.0, the ratio of the frictional coefficiencies to the fully developed flow coefficient starts at ~.8 at Ha/Re of ~$.5 \times 10^{-4}$ and gradually increases as Ha/Re increases. In the four meter channel preliminary analyses show that the ratio starts at a similar level at Ha/Re of .5, but decreases further as the Ha/Re ratio increases.

In summary, the data show that the frictional coefficients along the length of the thruster vary substantially and appear to be impacted strongly by operating conditions and channel design parameters.

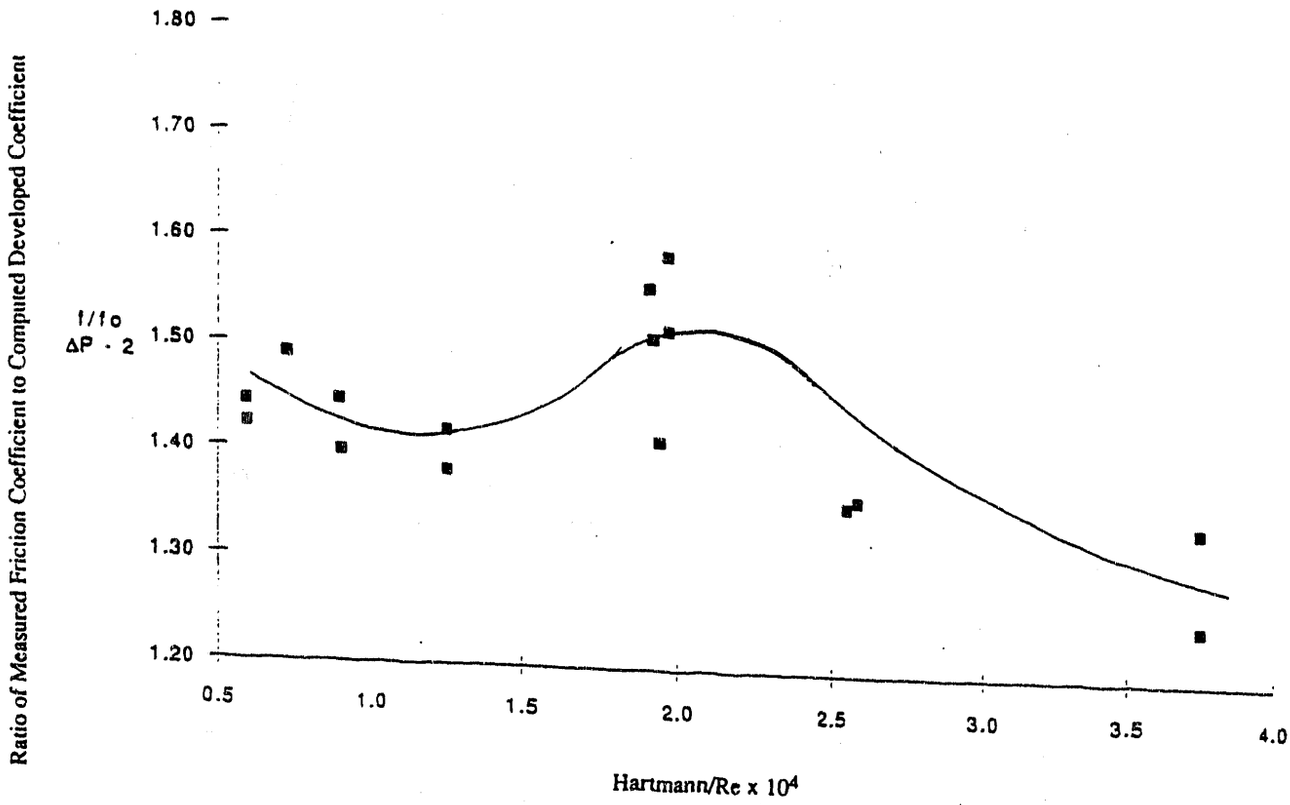

Figure 19.0 (f/fo vrs. Ht/Re, σ = 4.7, B = 6T, Run 502, L_T = 3M)

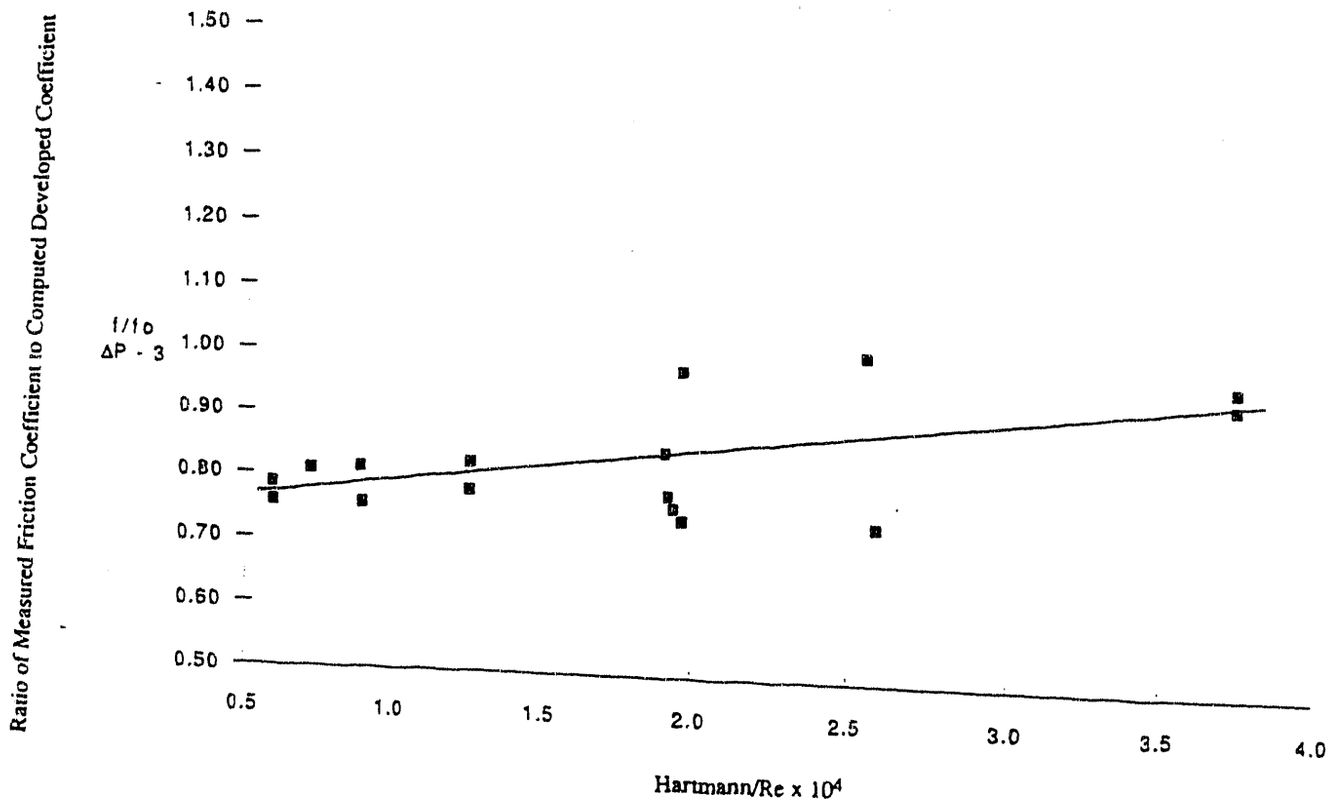

Figure 20.0 (f/fo vrs. Ht/Re, σ = 4.7, B = 6T, Run 502, L_T = 3M)

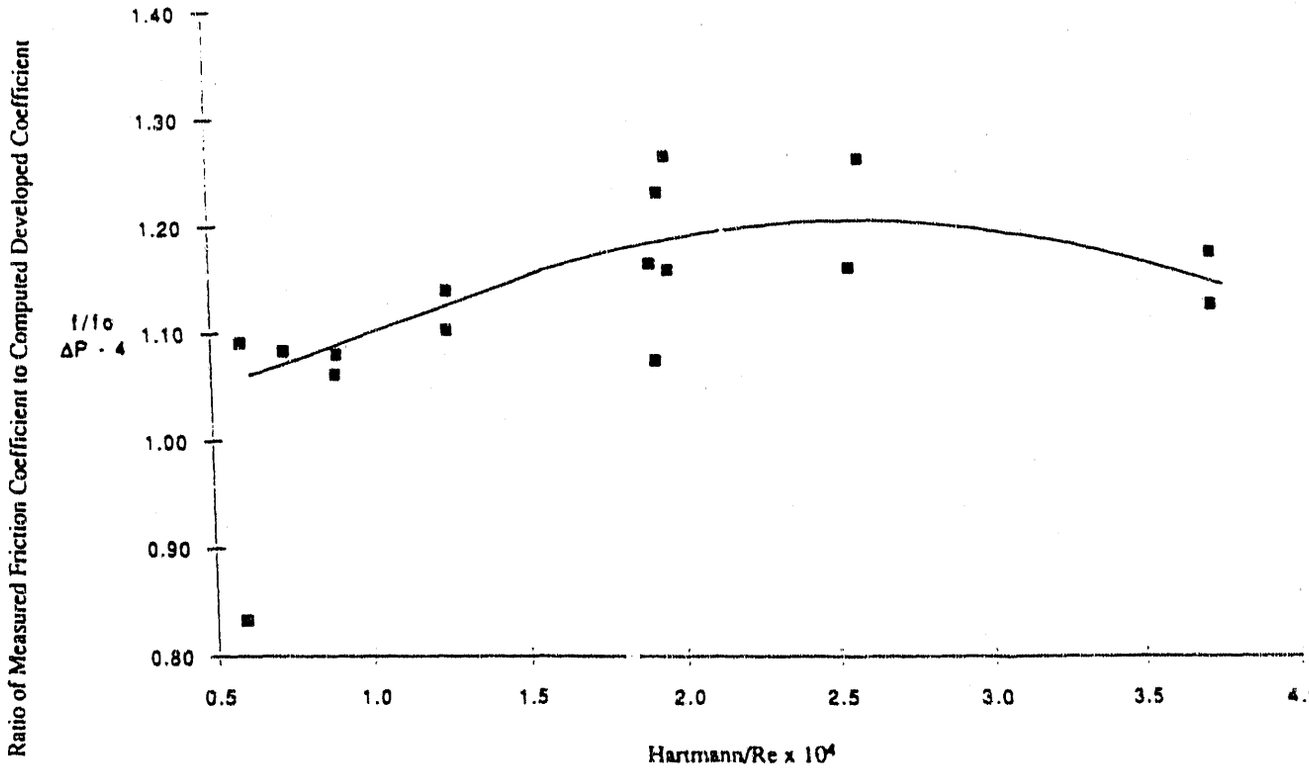

Figure 21.0 (f/fo vrs. Ht/Re, σ = 4.7, B = 6T, Run 502, L_T = 3M)

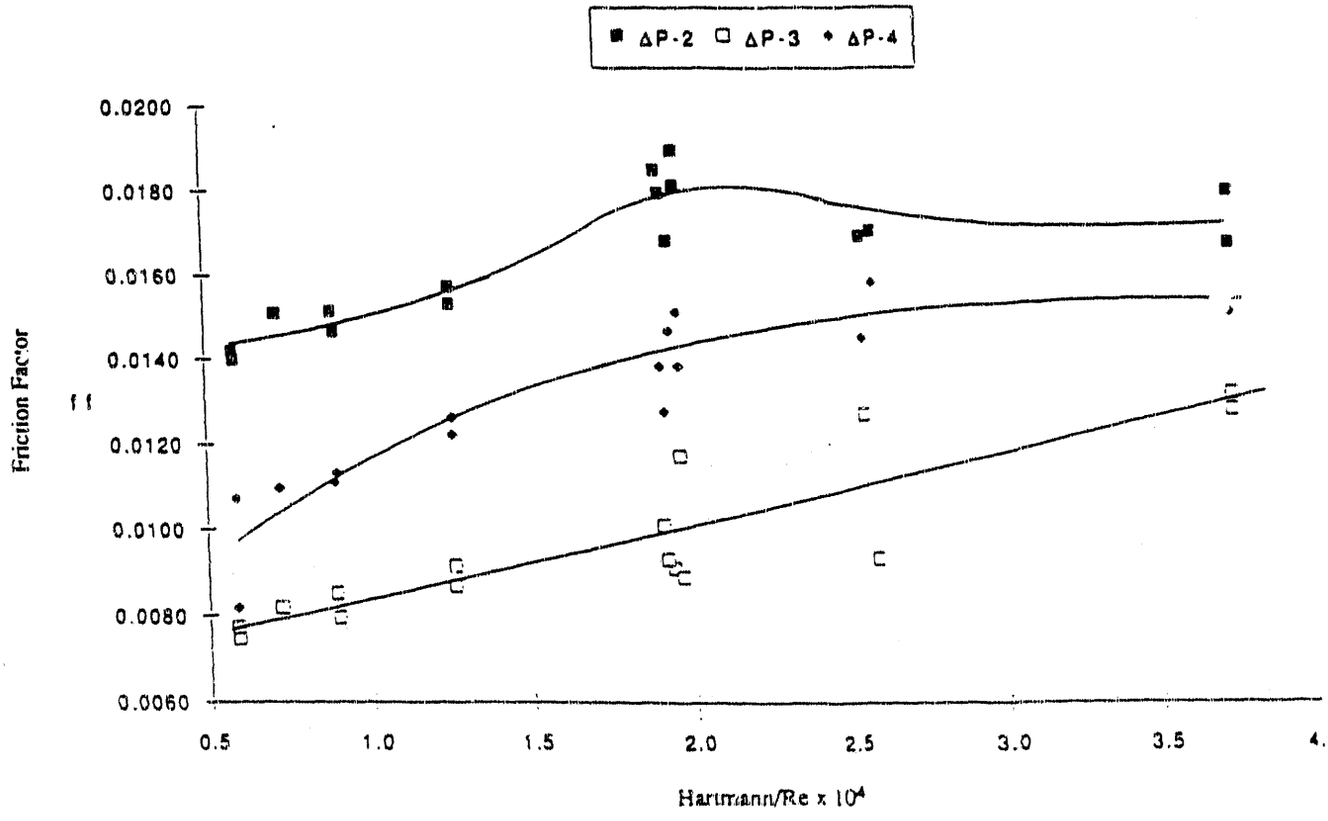

Figure 22.0 Friction Factor vrs. Ht/Re, σ = 4.7, B = 6T, L_T = 3M

SUMMARY

Typical data has been presented on this performance (efficiency) of sea water thrusters and on the magnitude of the individual loss mechanisms. The data are but a small fraction of the data base developed; data analyses is still continuing. The data support the position that efficient (60-75%) magnetohydrodynamic performance can be achieved, assuming the requisite magnet system (B>8T and SpWt $\leq$ 4 tons/m^3) can be developed and/or built. There appear to be no show stoppers from a magnetohydrodynamic viewpoint that would preclude MHD thruster development.

ACKNOWLEDGMENT

This work was supported by the Defense Advanced Research Projects Agency through an Interagency Agreement with the U.S. Department of Energy under contract No. W-31-109-ENG-38.

REFERENCES

1. Petrick, M., et al. "Magnetohydrodynamic Sea Water Propulsion", MHDS 91, Kobe, Japan, October (1991).

Approved for Public Release
Distribution Unlimited

DISCLAIMER

This report was prepared as an account of work sponsored by an agency of the United States Government. Neither the United States Government nor any agency thereof, nor any of their employees, makes any warranty, express or implied, or assumes any legal liability or responsibility for the accuracy, completeness, or usefulness of any information, apparatus, product, or process disclosed, or represents that its use would not infringe privately owned rights. Reference herein to any specific commercial product, process, or service by trade name, trademark, manufacturer, or otherwise does not necessarily constitute or imply its endorsement, recommendation, or favoring by the United States Government or any agency thereof. The views and opinions of authors expressed herein do not necessarily state or reflect those of the United States Government or any agency thereof.

END

DATE
FILMED
9/10/92